Nano Research
https://doi.org/10.1007/s12274-017-1812-z
Research Article
ISSN 1998-0124
CN 11-5974/O4

Semi-transparent polymer solar cells with all-copper nanowire electrodes

Haitao Zhai[1,2], Yang Li[3], Liwei Chen[3], Xiao Wang[1,2], Liangjing Shi[1], Ranran Wang[1] (✉), and Jing Sun[1] (✉)

[1] *the State Key Lab of High Performance Ceramics and Superfine Microstructure, Shanghai Institute of Ceramics, Chinese Academy of Sciences, Shanghai 200050, China*
[2] *University of Chinese Academy of Sciences, Beijing 100049, China*
[3] *Suzhou Institute of Nano-tech and Nano-bionics, Chinese Academy of Sciences, Suzhou 215123, China*

Received: 12 June 2017
Revised: 16 August 2017
Accepted: 20 August 2017

KEYWORDS
Cu nanowires,
transparent electrode,
semi-transparent polymer solar cells,
lamination

ABSTRACT

Transparent electrodes based on copper nanowires (Cu NWs) have attracted significant attention owing to their advantages including high optical transmittance, good conductivity, and excellent mechanical flexibility. However, low-cost, high-performance, and environmental friendly solar cells with all-Cu NW electrodes have not been realized until now. Herein, top and bottom transparent electrodes based on Cu NWs with low surface roughness and homogeneous conductivity are fabricated. Then, semi-transparent polymer solar cells (PSCs) with the inverted structure of polyacrylate/Cu NWs/poly(3,4-ethylenedioxythiophene):poly(styrenesulfonate) (PEDOT:PSS) (PH1000)/Y-TiO_2/poly(3-hexylthiophene):[6,6]-phenyl-C_{61}-butyric acid 3,4,5-tris(octyloxy)benzyl/PEDOT:PSS (4083)/Cu NWs/polyimide/polydimethylsiloxane are constructed; these could absorb light from both sides with a power conversion efficiency reaching 1.97% and 1.85%. Furthermore, the PSCs show an average transmittance of 42% in the visible region, which renders them suitable for some specialized applications such as power-generating windows and building-integrated photovoltaics. The indium tin oxide (ITO)- and noble metal-free PSCs could pave new pathways for fabricating cost-effective semi-transparent PSCs.

1 Introduction

Polymer solar cells (PSCs) have attracted significant attention in the past decade owing to their convenient fabrication, mechanical flexibility, and low cost [1–5]. In recent years, dramatic progress has been made with respect to the efficiency and versatile applications of PSCs, especially in the niche areas not applicable to Si-based solar cells [6–8]. Apart from the organic–bulk–heterojunction active layers, the electrodes, especially transparent electrodes which can significantly influence the device efficiency, cost, stability, and

Address correspondence to Jing Sun, jingsun@mail.sic.ac.cn; Ranran Wang, wangranran@mail.sic.ac.cn

mechanical flexibility are critical to the device performance. Indium tin oxide (ITO) is a popularly used transparent electrode material for PSCs. However, ITO electrodes have some drawbacks including the limited supply of indium, high cost, and fragility. Moreover, metal-based top electrodes used in PSCs also present some disadvantages such as the high cost of noble metals (e.g., Au and Ag) and poor chemical stability of Al. Therefore, low-cost electrode materials with excellent performance are in great demand for use in PSCs.

Recently, metal nanowires have been shown to demonstrate many advantages over conventional electrode materials used in solar cells, in terms of transparency, cost, mechanical flexibility, and encapsulation ability [9–13]. Many research groups have attempted to use metal nanowires as transparent anodes in organic solar cells. In 2010, Lee et al. [14] reported the application of silver nanowire (Ag NW) mesh as the top electrode of semi-transparent PSCs using the dry lamination method and demonstrated a power conversion efficiency of 0.63% with an average transmission of 26%. Krantz et al. [15] prepared semi-transparent PSCs using spray-coated Ag NWs as the top electrode and demonstrated their power conversion efficiency of 2.0%. Lu et al. [16] reported modified lamination of a Ag NW top electrode and its power conversion efficiency of 2.1%. Song et al. [17] prepared PSCs using solution-processed Ag NWs electrodes and obtained power conversion efficiencies comparable to those of the ITO-based devices. These studies presented the potential applications of Ag NWs as top and bottom electrodes. Compared to silver, copper presents a comparative conductivity but much lower cost and more abundant storage. Thus, replacing Ag NWs with copper nanowires (Cu NWs) should lead to comparable performance at a lower cost. However, the power conversion efficiencies of cells using Cu NWs electrodes are not as good as those using Ag NWs, so far. Chen et al. [18] prepared PSCs using solution-processed Cu NW electrodes and obtained a power conversion efficiency of 1.4%. Moreover, Cu NW-based top electrodes have not been reported. Although the optical and electrical performance of Cu NW electrodes are excellent, they present some inherent shortcomings such as the complicated post-treatment techniques required to obtain good electrical conductivity, inferior anti-corrosion stability, and high surface roughness. Many post-treatment methods have been developed [19–23], among which the most commonly used one is thermal annealing under the protection of H_2 or an inert gas, which however is not suitable for flexible substrates. The *in situ* polymerization method can effectively decrease the surface roughness of nanowire-based electrodes, because of the partial embedding of the nanowires in the polymer substrate. Unfortunately, conducting paths exposed on the surface are reduced because of the embedding, which is deleterious to charge collection and transfer.

In this study, semi-transparent PSCs with all-Cu NW electrodes (both an anode and cathode) are developed for the first time; these can absorb light from each side. H_2 plasma treatment was used to achieve excellent conductivity of the Cu NW network; this enables effective removal of the organic residues and surface oxides in few minutes at room temperature and induces plasmonic nanowelding at the inter-wire junctions at the same time. An *in situ* polymerization method was used to decrease the surface roughness of the Cu NW-based electrodes. Subsequently, a thin layer of poly(3,4-ethylenedioxythiophene):poly(styrenesulfonate) (PEDOT:PSS) was spin-coated to further smoothen the surface, as well as obtain homogeneous conducting paths. A lamination method was used to prepare the transparent Cu NW top electrode. In order to achieve excellent adhesion between the top electrode and active layer, a super-thin Cu NW/polyimide (PI)/polydimethylsiloxane (PDMS) top electrode (~80 μm) was prepared and an electronic glue was added to the PEDOT:PSS (4083) buffer layer. Eventually, semi-transparent PSCs based on poly(3- hexylthiophene) (P3HT) and [6,6]-phenyl-C_{61}-butyric acid 3,4,5-tris (octyloxy) benzyl ($PC_{61}BM$) with the inverted structure of polyacrylate (PA)/Cu NWs/PEDOT:PSS (PH1000)/Y-TiO_2/P3HT:$PC_{61}BM$/PEDOT:PSS (4083)/Cu NWs/PI/PDMS were successfully prepared and demonstrated to provide power convention efficiencies (PCE) up to 1.97% and 1.85% from each side, with an average transmittance of 42%. The low-cost semi- transparent device is promising for many emerging applications such as power-generating windows and roofs [24].

2 Experimental

2.1 Preparation of Cu NWs

For the synthesis of Cu NWs, we used a modified self-catalytic method which has been reported in our previous work [19, 25, 26]. In a typical process, 10 mL oleylamine (OA) and 0.5 g cetyl trimethyl ammonium bromide (CTAB) were dissolved in a glass vial at 180 ℃. Then, 200 mg of copper acetylacetonate ($Cu(acac)_2$) was added and mixed to obtain a homogeneous mixture. After that, 5–7 μL of a Pt nanoparticle suspension was added as the catalyst. The Pt nanoparticles were synthesized as follows: 2 mg of platinum chloride was dispersed in 1.2 mL ethylene glycol, and the mixture was added to 2.3 mL ethylene glycol preheated to 160 ℃ and maintained at this temperature for 90 s. The mixture was then heated up to 180 ℃ and allowed to react for 12 h, to yield reddish cotton-like sheets settled at the bottom. After rinsing several times with toluene, the nanowires were stored in toluene.

2.2 Preparation of Cu NWs transparent electrode

Typically, Cu NWs were dispersed in toluene via bath sonication for 1–2 min, and then filtered onto a nitrocellulose filter membrane. After filtration, the filter membrane was transferred to a glass slide, dried under vacuum at 80 ℃ for 2 h, and then dipped in acetone for 30 min to dissolve the filter membrane, leaving a Cu NW-based thin film on the glass slide. Finally, the films were treated by H_2 plasma to remove the oxide layers and the organic residues on the surface of the Cu NWs [27]. A liquid monomer of acrylate (SR601), which was fully mixed with a photo initiator, was dropped onto the surface of the Cu NW film and cured under ultraviolet (UV) irradiation [28]. Subsequently, the polyacrylate substrate electrode was peeled off from the glass slide. The thickness of the Cu NWs/PA composite electrode was controlled by a self-made mode. For the Cu NW-based anode (top electrode), a polyamic acid solution was spin-coated onto the Cu NW film and then baked to 360 ℃ to thermally imidize the polyamic acid. After baking, the transparent polyimide was peeled off, leaving a freestanding Cu NWs/PI electrode [29]. The thickness of the electrode depended on the velocity of rotation. The obtained Cu NWs/PI electrode was attached to a polydimethylsiloxane film (0.1 mm), washed four times with ethanol, and then treated with plasma for 60 s. After that, PEDOT:PSS (4083) mixed with *D*-sorbitol (0–250 mg/mL) was spin-coated on the Cu NW electrode, as a buffer layer. *D*-sorbitol acted as an electronic glue to improve the contact between PEDOT:PSS and the active layer [16].

2.3 Preparation of TiO_2 and Y-TiO_2

Titanium dioxide (TiO_2) and yttrium-doped titanium dioxide (Y-TiO_2) nanocrystals were prepared according to the method developed by Zhou et al. [30] In a typical synthesis, 0.5 mL $TiCl_4$ was slowly added to 2 mL ethanol with stirring, followed by the addition of 10 mL benzyl alcohol, resulting in a yellow solution. The solution was heated at 80 ℃ for 5 h, to obtain a slightly milky suspension. The suspension was mixed with 200 mL diethyl ether and centrifuged to collect the precipitate. The as-obtained product was re-dissolved in 30 mL absolute ethanol and precipitated via the addition of 200 mL diethyl ether. This procedure was repeated twice. The final TiO_2 nanoparticles were collected and dispersed in ethanol to obtain a suspension with a concentration of 3–6 mg/mL. The Y-TiO_2 nanocrystals were obtained following a similar approach except that YCl_3 was first dissolved in 2 mL ethanol. To stabilize the as-obtained TiO_2 and Y-TiO_2 suspensions, titanium oxide acetylacetonate $TiO(acac)_2$ was added to a final concentration of 15 μL/mL.

2.4 Fabrication of solar cells

An aqueous solution of PEDOT:PSS (Heraeus, Clevios PH1000) was spin-coated onto the Cu NWs/PA composite electrode at the speed of 1,000 rotations/min (r/min) for 60 s and annealed at 130 ℃ for 10 min. The thickness of the PEDOT:PSS layer after drying was ~150 nm. A thin layer of the TiO_2 (or Y-TiO_2) nanoparticles was spin-coated as the electron transfer layer. The substrate was then transferred to the glove-box, and a 70–200 nm thick photoactive layer was cast from 2.5 wt.% poly(3-hexylthiophene) (Rieke Metals): [6,6]-phenyl-C_{61}-butyric acid 3,4,5-tris(octyloxy)benzyl (American Dye Source) at a ratio of 1:0.8 in 1,2-dichlorobenzene [31]. After drying in a covered Petri

dish for ~120 min, the active layer was further annealed at 130 °C for 10 min to remove the solvent completely. Then, the device fabrication was completed by thermal evaporation of MoO_3 (10 nm) and Ag (100 nm) as the anode, under vacuum (2×10^{-3} Pa). For the semi-transparent polymer solar cells with all-Cu NW electrodes, the Cu NW-based anodes were laminated onto the active layer instead of the thermal evaporation of MoO_3 and Ag.

2.5 Characterization of samples

The TiO_2 and Y-TiO_2 nanocrystals were investigated by X-ray diffraction (XRD, D/max2550V, Rigaku Tokyo, Japan) and transmission electron microscopy (TEM, JEM-2100F, Japan), respectively. The morphology of the Cu NW-based electrode and the structure of the solar cells were characterized by field emission scanning electron microscopy (FESEM, Magellan 400, FEI, USA). Surface-resistivity was measured by a standard four-point probe method using a Loresta-EP MCP-T 360 instrument. The topological structures of the surface of the Cu NW-based electrode were obtained using an atomic force microscope (Dimension FastScan, Bruker, Germany). The transmittance of the electrodes and the semi-transparent cells was measured using the Lambda-950 UV-Vis spectrophotometer (PerkinElmer, Waltham, MA). Current density-voltage (*J*–*V*) characteristics of the solar cells were measured using an electrochemical work station (ModelCHI660C, CH) under AM 1.5G illumination (100 mW/cm^2, Model YSS-80A, Yamashita). The light source was Xe lamp equipped with an AM 1.5G filter. The intensity of the incident light was 100 mW/cm^2 calibrated with a standard Si solar cell. *J*–*V* curves were recorded by a Keithley Series 2400 System Source Meter Instrument in the stability test. A solar simulator (Newport) was used as the irradiation source to provide AM 1.5G illumination for the solar cells.

3 Results and discussion

To realize PSCs with all-Cu NW electrodes, Cu NW films with high conductivity and transparency are required. Cu NWs with a diameter of 60–80 nm and length over 50 μm were synthesized by a modified self-catalytic method which has been previously reported by our research team [19, 25]. Cu NW films were prepared by a vacuum filtration method and transferred onto PA substrates by *in situ* polymerization to decrease the surface roughness. In our experiments, to achieve an excellent conductivity of the Cu NW electrode, H_2 plasma treatment was used before the *in situ* polymerization [27]. The synthesis and transfer details can be found in the experimental section. Although the sheet resistance (R_s) of the Cu NWs decreases with an increase in the Cu NW density, a larger density of the Cu NWs leads to low transmittance and high surface roughness, which will influence the light absorbance and charge transfer in PSCs [32, 33]. Therefore, the sheet resistance of the Cu NW electrodes used in the following experiments was ~15 Ω/sq, and the average transmittance was about 85% at λ = 550 nm. To further improve the surface smoothness of the electrodes, a layer of PEDOT:PSS (thickness ~150 nm) was spin-coated. Figures 1(a) and 1(b) show the SEM images of the Cu NWs/PA electrode before and after spin-coating PEDOT:PSS. Some tilted Cu NWs can be observed on the surface of the electrode (marked in red circles), while a smooth surface was obtained after coating with PEDOT:PSS. The topological structures of the surface of the Cu NWs/PA electrode before and after spin-coating PEDOT:PSS are shown in Figs. 1(c) and 1(d). After coating PEDOT:PSS, the surface of the electrode became smoother and the surface roughness decreased from 4.82 to 3.28 nm. The conductivity distribution of the electrodes was measured by applying a voltage bias between the probe and sample. Figures 1(e) and 1(f) show the peak current of the electrode before and after coating PEDOT:PSS. The conductivity of the Cu NWs/PA electrode is inhomogeneous, which can be attributed to two aspects. First, the conducting paths of the nanowire-based electrodes are not as homogeneous as in film-based ones like ITO. Second, many nanowires were embedded in the polymer substrate after the *in situ* polymerization and transfer, which induced the inhomogeneity of the electrode. The conductance homogeneity was considerably improved after coating PEDOT:PSS. The smoother surface and more homogeneous conductivity of the composite electrode resulted in better performance of the solar cells than those reported in our previous work [27].

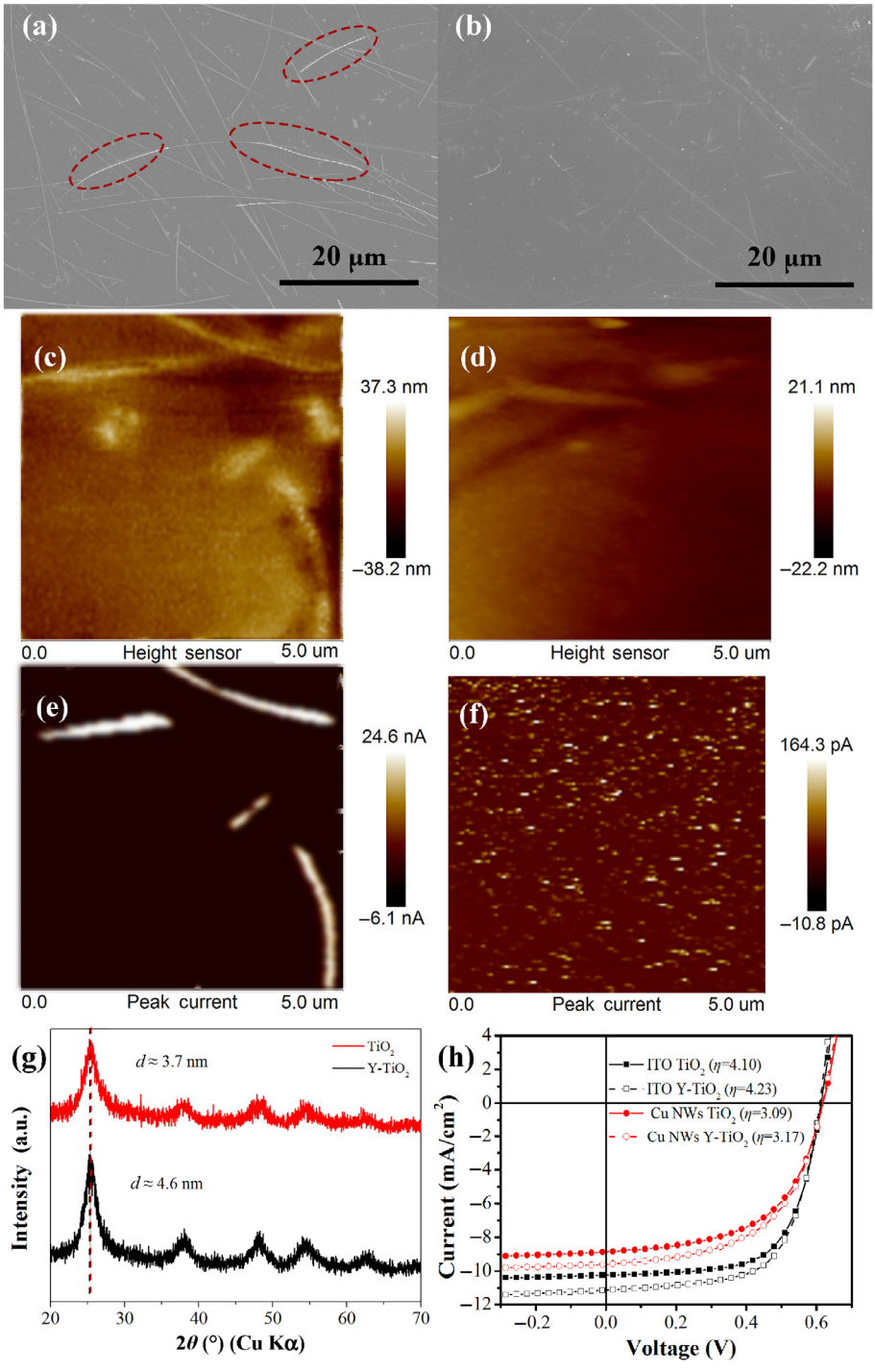

Figure 1 SEM images of Cu NWs/PA electrode before (a) and after (b) spin-coating of PEDOT:PSS. AFM images of the Cu NWs/PA electrode before (c), (e) and after (d), (f) spin-coating of PEDOT:PSS under height sensor (c), (d) and peak current (e), (f) modes. (g) X-ray diffraction patterns of the TiO_2 and Y-TiO_2 nanoparticles. (h) *J*–*V* curves of PSCs with different ETLs and bottom electrodes.

After spin-coating a thin layer (thickness: ~35 nm) of TiO_2 (or Y-TiO_2) nanoparticles as the electron transfer layer (ETL), the Cu NW-based electrode could be used as a transparent cathode in PSCs. Figure 1(g) shows the XRD patterns of the TiO_2 and Y-TiO_2 nanoparticles. All the diffraction peaks correlate with those of the pure anatase phase without the presence of any other polymorphs. The average crystallite sizes of the

powder samples were analyzed from the diffraction peaks, using the Scherrer formula [34]

$$d = 0.9\lambda / \omega \cos\theta \quad (1)$$

where d is the crystallite size, λ = 0.154 nm is the X-ray wavelength, ω is full width at half-maximum of the diffraction peak, and θ is the diffraction angle. The calculated results indicate that the particle sizes of the TiO_2 and Y-TiO_2 are 3.7 and 4.6 nm respectively, which are in good agreement with those observed in the TEM images (Fig. S1 in the Electronic Supplementary Material (ESM)).

Devices with the inverted structure of PA/Cu NWs/PEDOT:PSS/buffer layer/P3HT:$PC_{61}BM$/MoO_3/Ag were fabricated under optimized conditions. The current density–voltage (J–V) characteristics of the PSCs with different ETLs are shown in Fig. 1(h). The device based on Y-TiO_2 as the ETL showed a higher power conversion efficiency (PCE = 4.23%, open-circuit voltage (V_{OC}) = 0.61 V, short-circuit current density (J_{SC}) = 11.12 mA/cm^2, and fill factor (FF) = 62%) than the devices with TiO_2 (PCE = 4.10%) as the ETL, which can be mainly attributed to the enhanced electron extraction and transport performance of Y-TiO_2. For the cells based on PA/Cu NWs electrodes, a PCE of 3.17%, with V_{OC} = 0.62 V, J_{SC} = 9.27 mA/cm^2, and FF = 55%, was obtained when Y-TiO_2 was used as the ETL. This performance is superior to that of the device with TiO_2 as the ETL, which exhibited a PCE of 3.09%. Compared with ITO-based cells, the J_{SC} and FF of Cu NW-based cells are inferior, because of the relatively poor transmittance and higher surface roughness. With an improved technique and appropriate ETL, the PCE of our cells was more than doubled compared to that of the previously reported study (PCE = 1.4%, V_{OC} = 0.58 V, J_{SC} = 6.05 mA/cm^2, and FF = 40%) [13].

The thickness of active layer has a significant effect on the transmittance and PCE of the semi-transparent PSCs. It can be controlled easily by varying the spin-coating speed. Figures 2(a)–2(c) show the cross-sectional SEM images of the PSCs based on Cu NWs/PA electrodes with the rotational velocity used for spin-coating the active layer ranging from 600 to 1,200 r/min. The thickness of the PEDOT:PSS layer was about 150 nm, and the thickness of the Y-TiO_2 layer was about 35 nm. The thicknesses of the active layers with rotational velocities of 600, 900, and 1,200 r/min were about 200, 130, and 70 nm, respectively. The corresponding J-V curves of the devices with different thicknesses of the active layers are shown in Fig. 2(d).

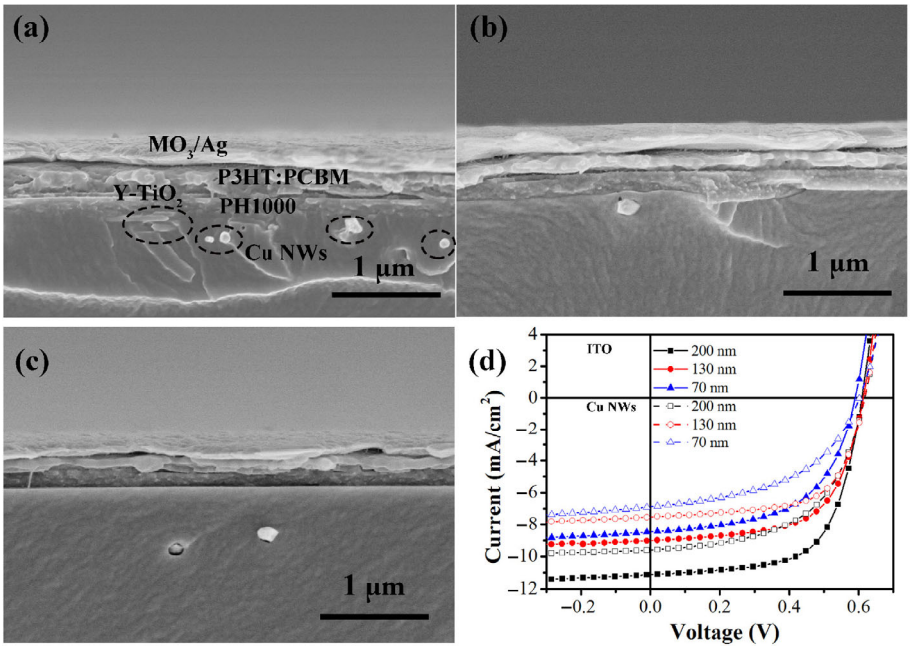

Figure 2 Cross-sectional SEM images of PSCs based on Cu NWs/PA electrodes with the spin-coating speed of the active layer of 600 (a), 900 (b), and 1,200 r/min (c). (d) J–V curve of PSCs based on ITO and Cu NW- electrodes with different thicknesses of active layers.

The photovoltaic parameters of the devices are summarized in Table 1. It is reasonable to observe that the J_{SC} and PCE values of the devices decreased with decreasing thickness of the active layer, because a thicker active layer can absorb and convert more luminous energy. The V_{OC} and PCE values decreased significantly when the thickness of the active layer was reduced to 70 nm. This is most likely due to the partial short-circuit of the device.

Furthermore, we prepared transparent Cu NW-based anodes and laminated them on inverted PSCs as top transparent electrodes. In order to ensure good contact between the top electrode and active layer, the substrate of the top electrode should be as thin and as flexible as possible. Herein, a polyamic acid solution was spin-coated onto the Cu NW film and baked to obtain highly flexible PI/Cu NWs transparent electrodes with a thickness of several tens of micrometers. Figures 3(a) and 3(b) present the SEM images of the Cu NWs/PI electrode before and after coating PEDOT:PSS (4083). The surface of the electrode became smoother after coating PEDOT:PSS. As shown in Fig. 3(c), the Cu NWs/PI film was stacked on a thin polydimethylsiloxane film (0.1 mm), making it convenient to be transferred and laminated on a conformal surface of a device. Then, the Cu NWs/PI/PDMS film was coated with a thin layer of PEDOT:PSS (4083). To improve the adhesion of the top electrode with the organic active layer during lamination, an effective electronic glue (*D*-sorbitol) used for organic optoelectronic devices was added in the PEDOT:PSS film at the concentration of 0–250 mg/mL. Then, the PEDOT:PSS/Cu NWs/PI/PDMS film was laminated on a P3HT:$PC_{61}BM$/Y-TiO_2/ITO device. Eventually, the device was encapsulated with an epoxy resin on the top [35]. It was obvious that the device was semi-transparent and could absorb light from both ITO and Cu NWs sides. The corresponding *J*–*V* curves of the semi-transparent device illuminated

Table 1 Photovoltaic parameters of PSCs based on ITO and Cu NWs electrodes with different thicknesses of the active layers

Velocity of rotation (r/min)/thickness	TEs	V_{OC} (V)	J_{SC} (mA/cm^2)	FF (%)	PCE (%)
600/200 nm	ITO	0.61	11.12	0.62	4.23
	Cu NWs	0.62	9.27	0.55	3.17
900/130 nm	ITO	0.62	8.98	0.62	3.44
	Cu NWs	0.62	7.45	0.61	2.81
1,200/70 nm	ITO	0.58	8.73	0.53	2.66
	Cu NWs	0.59	7.03	0.47	1.91

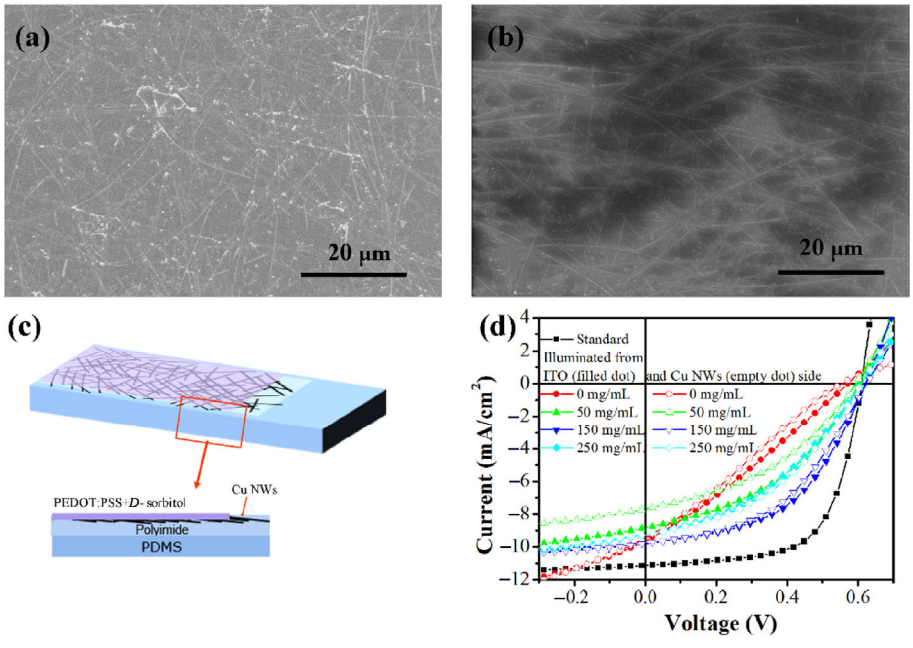

Figure 3 SEM images of Cu NWs/PI electrode before (a) and after (b) spin-coating with a PEDOT:PSS (4083) layer. Schematic (c) of a Cu NW anode with PEDOT:PSS as well as *D*-sorbitol modification of the surface. *J*–*V* curves (d) of the PSCs with different concentrations of *D*-sorbitol.

from the ITO or Cu NWs side are showed in Fig. 3(d). The photovoltaic parameters of the devices are summarized in Table 2. The best devices showed PCEs of 2.99% and 2.83% when illuminated from the ITO and Cu NWs side, respectively, with the *D*-sorbitol concentration of 150 mg/mL. These results are much better than the previously reported P3HT:$PC_{61}BM$-based semi-transparent solar cells based on Ag NWs (the best result of P3HT:$PC_{61}BM$-based cells with Ag NW top electrode ever reported: PCE = 2.1%, V_{OC} = 0.66 V, J_{SC} = 5.01 mA/cm^2, and FF = 63.6%) and graphene (the best result of P3HT:$PC_{61}BM$-based cells with graphene top electrode ever reported: PCE = 1.98%, V_{OC} = 0.58 V, J_{SC} = 10.40 mA/cm^2, and FF = 32.8%) electrodes [14–16, 36, 37]. For the cells without addition of *D*-sorbitol, PCE of 1.40% and 1.25% was obtained when illuminated from the ITO and Cu NWs sides, respectively. Compared with the best cells, the FF changed from 0.28 and 0.26 to 0.50 and 0.47 after adding an appropriate amount of *D*-sorbitol. This is due to the better adhesion of the top electrode on the organic active layer with the introduction of *D*-sorbitol. However, the performance of the cells was reduced with a higher concentration of *D*-sorbitol. It is interesting to observe that the device shows higher FF and PCE from the ITO side than from the Cu NWs side, which is possibly due to the better transmittance of ITO/Y-TiO_2 than Cu NWs/PEDOT:PSS.

Based on the above Cu NW cathode and anode, semi-transparent PSCs with all-Cu NW electrodes could be conveniently prepared using the procedure showed in Fig. 4. Inverted PSCs with both cathodes and anodes based on Cu NWs were prepared. Details of the fabrication are described in the experimental section. The transmittances of the semi-transparent PSCs with various active layer thicknesses were measured, and are shown in Fig. 5(a). The semi-transparent PSCs were dark red because the low-bandgap active layer can only absorb light with short wavelengths. The average transmittances of the semi-transparent PSCs with active layer thicknesses of 200, 130, and 70 nm are ~42%, 46%, and 48%, respectively, in the visible region. The high average transmittance of the device is due to the high transparency of the Cu NW electrodes and the weak absorption of the P3HT:$PC_{61}BM$ in the long wavelength range, rendering it suitable for some special applications. Figure 5(b) shows the *J*–*V* characteristics of the PSCs with various thicknesses of the active layers illuminated from either side. The related photovoltaic parameters are presented in Table 3. For the semi-transparent PSCs based on all-Cu NW electrodes with an average transmittance of 42%, PCE of 1.97% (1.85%), with V_{OC} = 0.62 V (0.62 V), J_{SC} = 7.08 mA/cm^2 (6.97 mA/cm^2), and FF = 0.45 (0.43) was obtained when illuminated from the top (bottom) Cu NWs electrode sides. Remarkably, the J_{SC} and PCE of the devices decreased with a reduction in the active layer thickness because a thicker active layer can absorb and convert more luminous energy. However, the V_{OC} and FF decreased

Table 2 Photovoltaic parameters of the semi-transparent PSCs with different concentration of *D*-sorbitol

	Illuminate from	V_{OC} (V)	J_{SC} (mA/cm^2)	FF (%)	PCE (%)
Standard		0.61	11.12	0.62	4.23
0 mg/mL	ITO side	0.57	8.74	0.28	1.40
	Cu NWs side	0.56	8.53	0.26	1.25
50 mg/mL	ITO side	0.60	8.83	0.41	2.20
	Cu NWs side	0.59	7.67	0.40	1.83
150 mg/mL	ITO side	0.62	10.24	0.50	2.99
	Cu NWs side	0.62	10.22	0.47	2.83
250 mg/mL	ITO side	0.61	8.80	0.42	2.23
	Cu NWs side	0.61	8.79	0.40	2.13

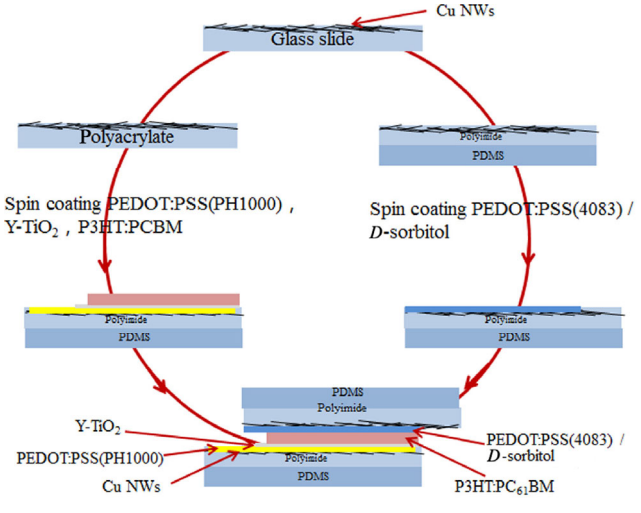

Figure 4 Schematic of the preparation procedure of PSCs with all-Cu NW electrodes.

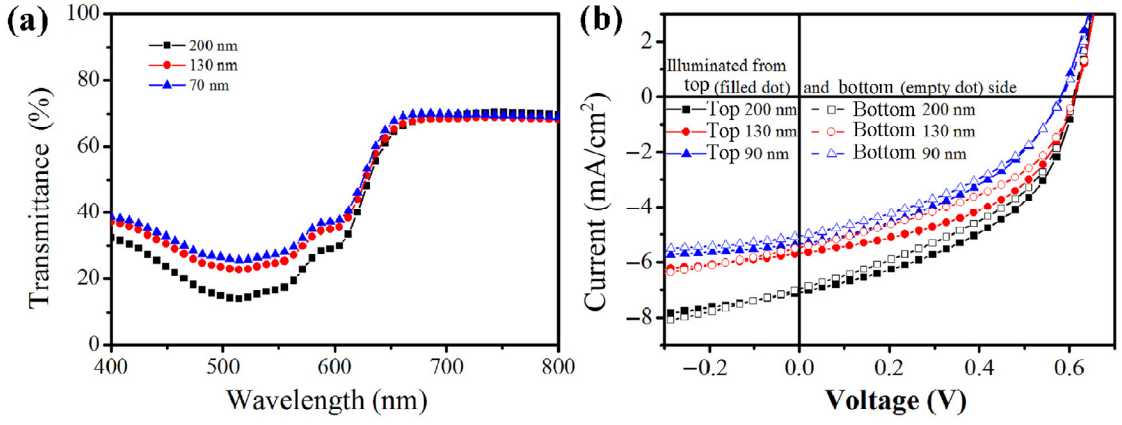

Figure 5 (a) Transmittance of the semi-transparent PSCs based on all-Cu NW electrode in the wavelength range of 400–800 nm. (b) *J*–*V* curves of the semi-transparent PSCs based on all-Cu NW electrode with different thickness of the active layer.

Table 3 Photovoltaic parameters of the semi-transparent PSCs based on all-Cu NW electrode with different thickness of the active layer

Velocity of rotation(r/min)/ thickness/ transmittance	Illuminate from	V_{OC} (V)	J_{SC} (mA/cm^2)	FF (%)	PCE (%)
600/200 nm/42%	Top Cu NWs	0.62	7.08	0.45	1.97
	Bottom Cu NWs	0.62	6.97	0.43	1.85
900/130 nm/46%	Top Cu NWs	0.62	5.68	0.46	1.62
	Bottom Cu NWs	0.62	5.52	0.43	1.47
1,200/70 nm/48%	Top Cu NWs	0.58	5.36	0.39	1.21
	Bottom Cu NWs	0.58	5.12	0.37	1.10

significantly when the thickness of the active layer was reduced to 70 nm, which is similar to the case in Fig. 2(d). The semi-transparent PSCs based on all-Cu NW electrodes showed higher FF and PCE from the top Cu NW electrodes than from the bottom ones, which is presumably due to the better transmittance of the top Cu NW electrode (with 35 nm PEDOT:PSS) than the bottom one (with 150 nm PEDOT:PSS).

4 Conclusions

In this work, an *in situ* polymerization method was used to decrease the surface roughness of Cu NW-based electrodes. A thin layer of poly(3,4-ethylene dioxythiophene):poly(styrenesulfonate) (PEDOT:PSS) was spin coated to further smoothen the surface as well as to obtain homogeneous conducting paths. A super thin Cu NWs/PI top electrode (~80 μm) was prepared and an electronic glue (150 mg/mL *D*-sorbitol) was added in the PEDOT:PSS (4083) buffer layer to obtain excellent adhesion between the top electrode and active layer for the lamination method. Semi-transparent PSCs with all-Cu NW electrodes were fabricated with an average transmittance of ~42% in the visible region and PCEs up to 1.97% and 1.85% from each side; these may find many potential applications such as power-generating windows and building-integrated photovoltaics. The devices can be conveniently prepared through film transfer, spin-coating, and lamination processes, indicating that the technique is compatible with the fabrication processes of other types of solar cells.

Acknowledgements

This work was financially supported by National Natural Science Foundation of China (No. 61301036), Shanghai Science and Technology Rising Star Project (No. 17QA1404700), Youth Innovation Promotion Association CAS (No. 2014226), Shanghai Key Basic Research Project (No. 16JC1402300), and the Major State Research Development Program of China (No. 2016YFA0203000).

Electronic Supplementary Material: Supplementary material (further details of the characterization of TiO_2 and Y-TiO_2) is available in the online version of this article at https://doi.org/10.1007/s12274-017-1812-z.

References

[1] Tang, C. W. Two-layer organic photovoltaic cell. *Appl. Phys. Lett.* **1986**, *48*, 183–185.

[2] Granström, M.; Petritsch, K.; Arias, A. C.; Lux, A.; Andersson, M. R.; Friend, R. H. Laminated fabrication of polymeric photovoltaic diodes. *Nature* **1998**, *395*, 257–260.

[3] He, Z. C.; Zhong, C. M.; Su, S. J.; Xu, M.; Wu, H. B.; Cao, Y. Enhanced power-conversion efficiency in polymer solar cells using an inverted device structure. *Nat. Photonics* **2012**, *6*, 591–595.

[4] Kim, J.; Hong, Z. R.; Li, G.; Song, T. B.; Chey, J.; Lee, Y. S.; You, J. B.; Chen, C. C.; Sadana, D. K.; Yang, Y. 10.5% efficient polymer and amorphous silicon hybrid tandem photovoltaic cell. *Nat.Commun.* **2015**, *6*, 6391.

[5] Chen, J. D.; Cui, C. H.; Li, Y. Q.; Zhou, L.; Ou, Q. D.; Li, C.; Li, Y. F.; Tang, J. X. Single-junction polymer solar cells exceeding 10% power conversion efficiency. *Adv. Mater.* **2015**, *27*, 1035–1041.

[6] Kaltenbrunner, M.; White, M. S.; Glowacki, E. D.; Sekitani, T.; Someya, T.; Sariciftci, N. S.; Bauer, S. Ultrathin and lightweight organic solar cells with high flexibility. *Nat. Commun.* **2012**, *3*, 770.

[7] You, J. B.; Dou, L. T.; Yoshimura, K.; Kato, T.; Ohya, K.; Moriarty, T.; Emery, K.; Chen, C. C.; Gao, J.; Li, G. et al. A polymer tandem solar cell with 10.6% power conversion efficiency. *Nat. Commun.* **2013**, *4*, 1446.

[8] Liu, Y. H.; Zhao, J. B.; Li, Z. K.; Mu, C.; Ma, W.; Hu, H. W.; Jiang, K.; Lin, H. R.; Ade, H.; Yan, H. Aggregation and morphology control enables multiple cases of high-efficiency polymer solar cells. *Nat. Commun.* **2014**, *5*, 5293.

[9] Angmo, D.; Andersen, T. R.; Bentzen, J. J.; Helgesen, M.; Søndergaard, R. R.; Jørgensen, M.; Carlé, J. E.; Bundgaard, E.; Krebs, F. C. Roll-to-roll printed silver nanowire semitransparent electrodes for fully ambient solution-processed tandem polymer solar cells. *Adv. Funct. Mater.* **2015**, *25*, 4539–4547.

[10] Wu, J.; Que, X. L.; Hu, Q.; Luo, D. Y.; Liu, T. H.; Liu, F.; Russell, T. P.; Zhu, R.; Gong, Q. H. Organic solar cells: Multi-length scaled silver nanowire grid for application in efficient organic solar cells. *Adv. Funct. Mater.* **2016**, *26*, 4806.

[11] Kim, Y.; Ryu, T. I.; Ok, K. H.; Kwak, M. G.; Park, S.; Park, N. G.; Han, C. J.; Kim, B. S.; Ko, M. J.; Son, H. J. et al. Inverted layer-by-layer fabrication of an ultraflexible and transparent Ag nanowire/conductive polymer composite electrode for use in high-performance organic solar cells. *Adv. Funct. Mater.* **2015**, *25*, 4743.

[12] Stewart, I. E.; Rathmell, A. R.; Yan, L.; Ye, S. R.; Flowers, P. F.; You, W.; Wiley, B. J. Solution-processed copper-nickel nanowire anodes for organic solar cells. *Nanoscale* **2014**, *6*, 5980–5988.

[13] Sachse, C.; Weiß, N.; Gaponik, N.; Müller-Meskamp, L.; Eychmüller, A.; Leo, K. ITO-free, small-molecule organic solar cells on spray-coated copper-nanowire-based transparent electrodes. *Adv. Energy Mater.* **2014**, *4*, 1300737.

[14] Lee, J. Y.; Connor, S. T.; Cui, Y.; Peumans, P. Semitransparent organic photovoltaic cells with laminated top electrode. *Nano Lett.* **2010**, *10*, 1276–1279.

[15] Krantz, J.; Stubhan, T.; Richter, M.; Spallek, S.; Litzov, I.; Matt, G. J.; Spiecker, E.; Brabec, C. J. Spray-coated silver nanowires as top electrode layer in semitransparent P3HT:PCBM-based organic solar cell devices. *Adv. Funct. Mater.* **2013**, *23*, 1711–1717.

[16] Lu, H. F.; Zhang, D.; Ren, X. G.; Liu, J.; Choy, W. C. H. Selective growth and integration of silver nanoparticles on silver nanowires at room conditions for transparent nanonetwork electrode. *ACS Nano* **2014**, *8*, 10980–10987.

[17] Song, M.; You, D. S.; Lim, K.; Park, S.; Jung, S.; Kim, C. S.; Kim, D. H.; Kim, D. G.; Kim, J. K.; Park, J. et al. Highly efficient and bendable organic solar cells with solution-processed silver nanowire electrodes. *Adv. Funct. Mater.* **2013**, *23*, 4177–4184.

[18] Chen, J. Y.; Zhou, W. X.; Chen, J.; Fan, Y.; Zhang, Z. Q.; Huang, Z. D.; Feng, X. M.; Mi, B. X.; Ma, Y. W.; Huang, W. Solution-processed copper nanowire flexible transparent electrodes with PEDOT:PSS as binder, protector and oxide-layer scavenger for polymer solar cells. *Nano Res.* **2015**, *8*, 1017–1025.

[19] Zhang, D. Q.; Wang, R. R.; Wen, M. C.; Weng, D.; Cui, X.; Sun, J.; Li, H. X.; Lu, Y. F. Synthesis of ultralong copper nanowires for high-performance transparent electrodes. *J. Am. Chem. Soc.* **2012**, *134*, 14283–14286.

[20] Han, S.; Hong, S.; Ham, J.; Yeo, J.; Lee, J.; Kang, B.; Lee, P.; Kwon, J.; Lee, S. S.; Yang, M. Y. et al. Flexible electronics: Fast plasmonic laser nanowelding for a cu-nanowire percolation network for flexible transparent conductors and stretchable electronics. *Adv. Mater.* **2014**, *26*, 5888.

[21] Zhong, Z. Y.; Lee, H.; Kang, D.; Kwon, S.; Choi, Y. M.; Kim, I.; Kim, K. Y.; Lee, Y.; Woo, K.; Moon, J. Continuous patterning of copper nanowire-based transparent conducting electrodes for use in flexible electronic applications. *ACS Nano* **2016**, *10*, 7847–7854.

[22] Mayousse, C.; Celle, C.; Carella, A.; Simonato, J. P. Synthesis and purification of long copper nanowires. Application to high performance flexible transparent electrodes with and without PEDOT:PSS. *Nano Res.* **2014**, *7*, 315–324.

[23] Wang, X.; Wang, R. R.; Zhai, H. T.; Shen, X.; Wang, T.; Shi, L. J.; Yu, R. C.; Sun, J. Room-temperature surface

modification of cu nanowires and their applications in transparent electrodes, SERS-based sensors, and organic solar cells. *ACS Appl. Mater. Interfaces* **2016**, *8*, 28831–28837.

[24] Chen, K. S.; Salinas, J. F.; Yip, H. L.; Huo, L. J.; Hou, J. H.; Jen, A. K. Y. Semi-transparent polymer solar cells with 6% PCE, 25% average visible transmittance and a color rendering index close to 100 for power generating window applications. *Energy Environ. Sci.* **2012**, *5*, 9551–9557.

[25] Zhai, H. T.; Wang, R. R.; Wang, W. Q.; Wang, X.; Cheng, Y.; Shi, L. J.; Liu, Y. Q.; Sun, J. Novel fabrication of copper nanowire/cuprous oxidebased semiconductor-liquid junction solar cells. *Nano Res.* **2015**, *8*, 3205–3215.

[26] Cheng, Y.; Wang, R. R.; Sun, J.; Gao, L. A stretchable and highly sensitive graphene-based fiber for sensing tensile strain, bending, and torsion. *Adv. Mater.* **2015**, *27*, 7365–7371.

[27] Wang, R. R.; Zhai, H. T.; Wang, T.; Wang, X.; Cheng, Y.; Shi, L. J.; Sun, J. Plasma-induced nanowelding of a copper nanowire network and its application in transparent electrodes and stretchable conductors. *Nano Res.* **2016**, *9*, 2138–2148.

[28] Wang, S. L.; Cheng, Y.; Wang, R. R.; Sun, J.; Gao, L. Highly thermal conductive copper nanowire composites with ultralow loading: Toward applications as thermal interface materials. *ACS Appl. Mater. Interfaces* **2014**, *6*, 6481–6486.

[29] Spechler, J. A.; Koh, T. W.; Herb, J. T.; Rand, B. P.; Arnold, C. B. A transparent, smooth, thermally robust, conductive polyimide for flexible electronics. *Adv. Funct. Mater.* **2015**, *25*, 7428–7434.

[30] Zhou, H. P.; Chen, Q.; Li, G.; Luo, S.; Song, T. B.; Duan, H. S.; Hong, Z. R.; You, J. B.; Liu, Y. S.; Yang, Y. Interface engineering of highly efficient perovskite solar cells. *Science* **2014**, *345*, 542–546.

[31] Mao, L.; Chen, Q.; Li, Y. W.; Li, Y.; Cai, J. H.; Su, W. M.; Bai, S.; Jin, Y. Z.; Ma, C. Q.; Cui, Z. et al. Flexible silver grid/PEDOT:PSS hybrid electrodes for large area inverted polymer solar cells. *Nano Energy* **2014**, *10*, 259–267.

[32] Wang, Y.; Tong, S. W.; Xu, X. F.; Öezyilmaz, B.; Loh, K. P. Interface engineering of layer-by-layer stacked graphene anodes for high-performance organic solar cells. *Adv. Mater.* **2011**, *23*, 1514–1518.

[33] Park, H.; Brown, P. R.; Buloyić, V.; Kong, J. Graphene as transparent conducting electrodes in organic photovoltaics: studies in graphene morphology, hole transporting layers, and counter electrodes. *Nano Lett.* **2012**, *12*, 133–140.

[34] Wang, J.; Polleux, J.; Lim, J.; Dunn, B. Pseudocapacitive contributions to electrochemical energy storage in TiO_2 (anatase) nanoparticles. *J. Phys. Chem. C* **2007**, *111*, 14925–14931.

[35] Liu, Z. K.; You, P.; Liu, S. H.; Yan, F. Neutral-color semitransparent organic solar cells with all-graphene electrodes. *ACS Nano* **2015**, *9*, 12026–12034.

[36] Liu, Z. K.; Li, J. H.; Sun, Z. H.; Tai, G. A.; Lau, S. P.; Yan, F. The application of highly doped single-layer graphene as the top electrodes of semitransparent organic solar cells. *ACS Nano* **2012**, *6*, 810–818.

[37] Park, H.; Chang, S.; Smith, M.; Gradečak, S.; Kong, J. Interface engineering of graphene for universal applications as both anode and cathode in organic photovoltaics. *Sci. Rep.* **2013**, *3*, 1581.